Supporting Information for

Improved Slow Magnetic Relaxation in Optically Pure Helicene-Based Dy^{III} Single Molecule Magnet

Jiang-Kun Ou-Yang,[1] Nidal Saleh,[1] Guglielmo Fernandez Garcia,[1,2] Lucie Norel,[1] Fabrice Pointillart,[*,1] Thierry Guizouarn,[1] Olivier Cador,[1] Federico Totti,[2] Lahcène Ouahab,[1] Jeanne Crassous,[*,1] and Boris Le Guennic[*,1]

[1] Institut des Sciences Chimiques de Rennes, UMR 6226 CNRS - Université de Rennes 1, 263 Avenue du Général Leclerc 35042 Rennes Cedex (France)

[2] Department of Chemistry "Ugo Schiff" and INSTM RU, University of Florence, 50019 Sesto Fiorentino (Italy)

Experimental section

General Procedures and Materials.

The precursors $Dy(hfac)_3{\cdot}2H_2O$[1] ($hfac^-$ = 1,1,1,5,5,5-hexafluoroacetonate anion), racemic (**L**) and optically pure 3-(2-pyridyl)-4-aza[6]-helicene[2] (**L(-)** and **L(+)**) were synthesized following previously reported methods. All other reagents were purchased from Aldrich Co., Ltd. and used without further purification.

Synthesis of complexes

$[Dy(hfac)_3(L)]{\cdot}0.5C_6H_{14}$ (*rac*-1$\cdot$0.5C_6H_{14}). $Dy(hfac)_3{\cdot}2H_2O$ (16.4 mg, 0.02 mmol) were dissolved in 5 mL of CH_2Cl_2 and then added to a solution of 5 mL of CH_2Cl_2 containing 8.3 mg of **L** (0.02 mmol). After 20 minutes of stirring, 35 mL of *n*-hexane were layered at room temperature in the dark. Slow diffusion leads to yellow single crystals which are suitable for X-ray studies. Yield: 17.5 mg (71 %). Anal. Calcd (%) for $C_{48}H_{28}DyF_{18}N_2O_6$: C 46.71, H 2.27, N 2.27; found: C 46.59, H 2.16 N, 2.29.

[Dy(hfac)$_3$(L(-))] (**1**(-)) and **[Dy(hfac)$_3$(L(+))]** (**1**(+)). The same experimental protocol than for the racemic complex is used except than **L**(-) and **L**(+) were used instead of **L**. Slow diffusions following by slow evaporations lead to light yellow single crystals which are suitable for X-ray studies. Yield: 15.5 mg (65 %) and 16.2 mg (68 %) respectively for **1**(-) and **1**(+). Anal. Calcd (%) for $C_{45}H_{21}DyF_{18}N_2O_6$: C 45.37, H 1.76, N 2.35; found: C 45.39, H 1.81, N 2.38.

Crystallography. Single crystals of *rac*-**1**·0.5C_6H_{14}, **1**(-) and **1**(+) were mounted on a APEXII Bruker-AXS diffractometer (MoK_α radiation source, λ = 0.71073 Å, T = 150(2) K) for data collection, from the Centre de Diffractométrie (CDIFX), Université de Rennes 1, France. Structures were solved with a direct method using the SIR-97 program and refined with a full matrix least-squares method on F^2 using the SHELXL-97 program[3] for all the compounds. Crystallographic data are summarized in Table S1. Complete crystal structure results as a CIF file including bond lengths, angles, and atomic coordinates are deposited as Supporting Information.

Physical Measurements. The elementary analyses of the compounds were performed at the Centre Régional de Mesures Physiques de l'Ouest, Rennes. Specific rotations (in deg cm^2 g^{-1}) were measured in a 1 dm thermostated quartz cell on a Perkin–Elmer- 341 polarimeter. Circular dichroism (in M^{-1} cm^{-1}) was measured on a Jasco J-815 Circular Dichroism Spectrometer (IFR140 facility, Biosit platform, Université de Rennes 1). The dc magnetic susceptibility measurements were performed on solid polycrystalline sample with a Quantum Design MPMS-XL SQUID magnetometer between 2 and 300 K in an applied magnetic field of 200 Oe in the 2-20 K temperature range, 2 kOe between 20 and 80 K and 10 kOe above. These measurements were all corrected from the diamagnetic contribution of the sample holder as well as the intrinsic diamagnetism calculated with Pascal's constants. Ac measurements are performed with 3 Oe oscillating field amplitude. Hysteresis loops at 500 mK have been recorded with the help of a ^{3}He insert (iHelium3) adapted to SQUID magnetometer. The magnetic field is then swept in hysteresis mode and the magnetic moment measured with RSO head. The sweep rate is estimated to be close to 16 Oe s^{-1}. The dc and ac magnetic susceptibility of the dichloromethane solution have been measured with a modified NMR tube containing 0.2 mL of solution of concentration 6 mM. The ac data were corrected from the diamagnetism of dichloromethane and from the sample holder.

Computational Details. Wavefunction-based calculations were carried out on molecular structures of the Dy^{III}-based complexes *rac*-**1** and **1(+)** by using the SA-CASSCF/RASSI-SO approach, as implemented in the MOLCAS quantum chemistry package (versions 8.0).[4] In this approach, the relativistic effects are treated in two steps on the basis of the Douglas–Kroll Hamiltonian. First, the scalar terms were included in the basis-set generation and were used to determine the spin-free wavefunctions and energies in the complete active space self-consistent field (CASSCF) method.[5] Next, spin-orbit coupling was added within the restricted-active-space-state-interaction (RASSI-SO) method, which uses the spin-free wavefunctions as basis states.[6] The resulting wavefunctions and energies are used to compute the magnetic properties and g-tensors of the lowest states from the energy spectrum by using the pseudo-spin $S = 1/2$ formalism in the SINGLE-ANISO routine.[7] Cholesky decomposition of the bielectronic integrals was employed to save disk space and speed-up the calculations.[8] For *rac*-**1** and **1(+)**, the active space of the self consistent field (CASSCF) method consisted of the nine 4f electrons of the Dy^{III} ion spanning the seven 4f orbitals, i.e. CAS(9,7)SCF. State-averaged CASSCF calculations were performed for all of the sextets (21 roots), all of the quadruplets (224 roots), and 300 out of the 490 doublets (due to software limitations) of the Dy^{III} ion. Twenty-one sextets, 128 quadruplets, and 107 doublets were mixed through spin−orbit coupling in RASSI-SO. All atoms were described by ANO-RCC basis sets.[9] The following contractions were used: [8s7p4d3f2g1h] for Dy, [4s3p2d] for the O and N atoms,,[3s2p] for the C and F atoms and [2s] for the H atoms. The atomic positions were extracted from the X-ray crystal structures. Only the position of the H atoms were optimized on the Y^{III} parent complexes with the Gaussian 09 (revision D.01) package[10] employing the PBE0 hybrid functional.[11] The "Stuttgart/Dresden" basis sets and effective core potentials were used to describe the yttrium atom,[12] whereas all other atoms were described with the SVP basis sets.[13]

For the calculation of the isotropic dipolar coupling between two molecules we employed the following formula:[14]

$$J_{dip}^{12} = \frac{1}{3} Tr\left\{ \frac{\mu_B^2}{R_{12}^3} \left(g_1 \cdot g_2 - 3 \left(g_1 \cdot R_{12} \right) \left(R_{12} \cdot g_2 \right) \right) \right\}$$

where g_1 and g_2 are the *g*-tensors calculated *ab initio*, R_{12} is the distance vector between two Dy^{III} atoms and $\hat{I}_{-B}$ is the Bohr magneton. Since J_{dip} is proportional to R_{12}^{-3} , we only took into account the first neighbors to calculate the average coupling values. Figures S10 and S11 show the schematics maps of the dipolar couplings in the crystal structures. The

corresponding J_{dip} for each couple are collected in Table S5. The temperature dependence of $\chi_M T$ accounting for the average J_{dip} were calculated with the SINGLE_ANISO routine.

Table S1. X-ray crystallographic data for the complexes **1**·0.5C_6H_{14}, **1(-)** and **1(+)**.

Compounds	$[Dy(hfac)_3(\mathbf{L})]\cdot 0.5C_6H_{14}$ *rac*-**1**·0.5C_6H_{14}	$[Dy(hfac)_3(\mathbf{L(-)})]$ **1(-)**	$[Dy(hfac)_3(\mathbf{L(+)})]$ **1(+)**
Formula M / g.mol^{-1}	$C_{48}H_{28}DyF_{18}N_2O_6$ 1233.22	$C_{45}H_{21}DyF_{18}N_2O_6$ 1190.14	$C_{45}H_{21}DyF_{18}N_2O_6$ 1190.14
Crystal system	Triclinic	Orthorhombic	Orthorhombic
Space group	P-1 (N°2)	$P2_12_12_1$ (N°19)	$P2_12_12_1$ (N°19)
Cell parameters	a = 13.2160(5) Å b = 13.9132(6) Å c = 14.5959(6) Å α = 67.984(2) ° β = 72.454(2) ° γ = 84.724(17) °	a = 11.1191(9) Å b = 17.6604(18) Å c = 22.693(2) Å	a = 11.1110(6) Å b = 17.6697(12) Å c = 22.3965(14) Å
Volume / Å^3	2371.7(2)	4456.2(7)	4456.0(5)
Z	2	4	4
T / K	150 (2)	150(2)	150(2)
2θ range / °	$3.14 \leq 2\theta \leq 54.92$	$2.92 \leq 2\theta \leq 54.98$	$2.92 \leq 2\theta \leq 54.96$
ρ_{calc} / g.cm^{-3}	1.727	1.774	1.774
μ / mm^{-1}	1.698	1.804	1.804
Number of reflections	38886	25548	15348
Independent reflections	10755	10112	9283
R_{int}	0.0258	0.1334	0.0265
$Fo^2 > 2\sigma(Fo)^2$	9745	5232	8235
Number of variables	701	608	649
R_1, wR_2	0.0369, 0.1012	0.0814, 0.1666	0.0377, 0.0803

Table S2. SHAPE analysis of the coordination polyhedron around the Dy^{III} ion in *rac*-**1**·0.5C_6H_{14}, **1(-)** and **1(+)**.

	$CShM_{SAPR-8}$ (square antiprism) D_{4d}	$CShM_{BTPR-8}$ (biaugmented trigonal prism) C_{2v}	$CShM_{TDD-8}$ (triangular dodecahedron) D_{2d}
rac-**1**	1.613	2.288	0.784
1(-)	2.429	2.081	0.504
1(+)	2.348	2.057	0.486

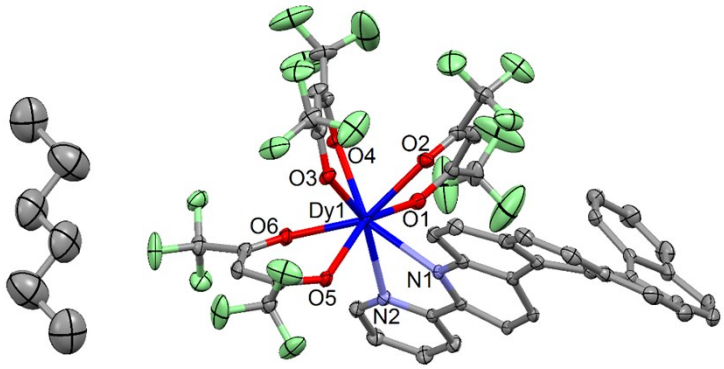

Figure S1. ORTEP view of the asymmetric unit for *rac*-**1**·0.5C_6H_{14}. Thermal ellipsoids are drawn at 30% probability. Hydrogen atoms are omitted for clarity.

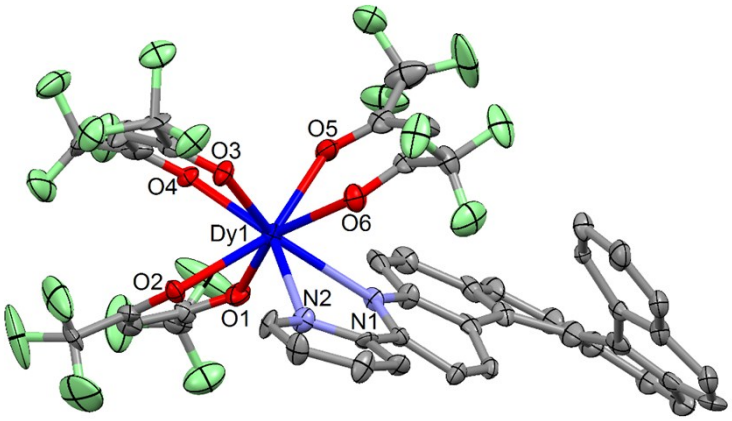

Figure S2. ORTEP view of the asymmetric unit for **1(-)**. Thermal ellipsoids are drawn at 30% probability. Hydrogen atoms are omitted for clarity.

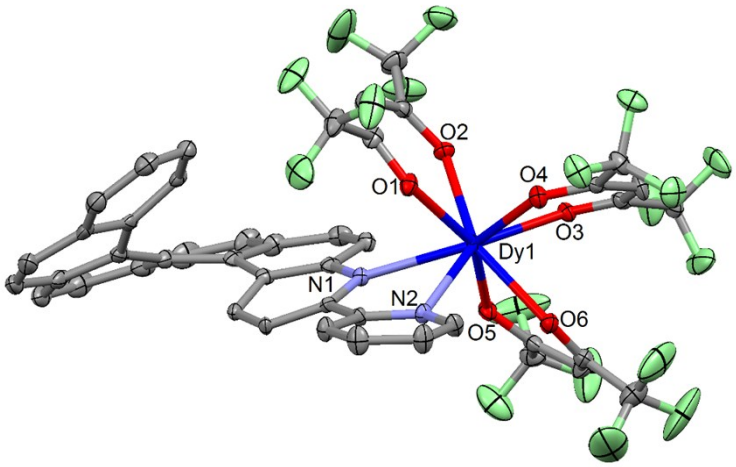

Figure S3. ORTEP view of the asymmetric unit for **1(+)**. Thermal ellipsoids are drawn at 30% probability. Hydrogen atoms are omitted for clarity.

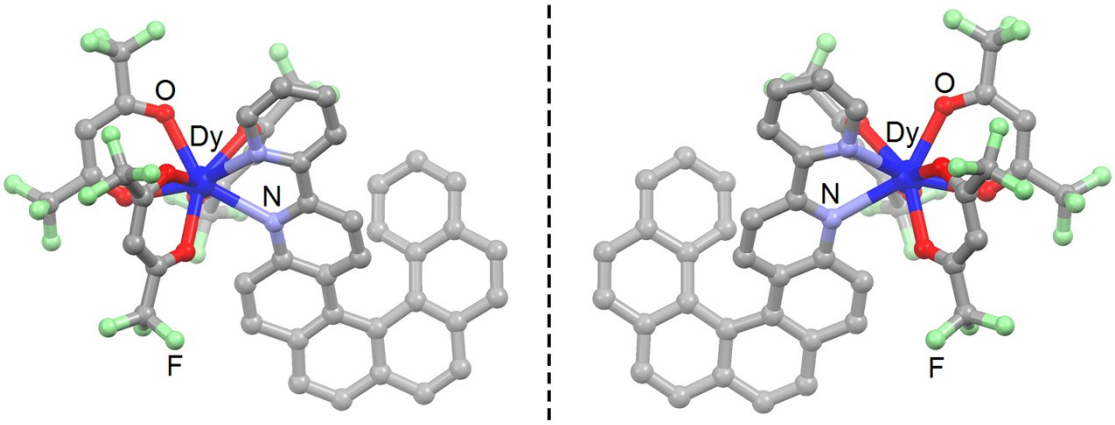

Figure S4. Molecular structures of **1(-)** (left) and **1(+)** (right) complexes. The dash line represents the mirror between both enantiomers. H atoms are omitted for sake of clarity.

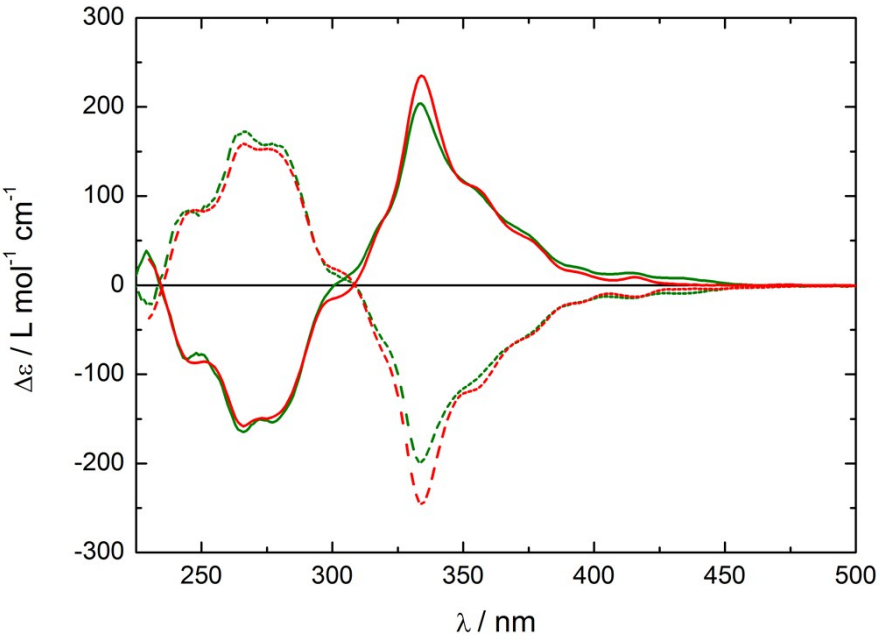

Figure S5. Experimental (CH_2Cl_2, ca. 5×10^{-5} M) ECD spectra of enantiopure **L(-)** (dash red line) and **L(+)** (full red line) and respective Dy^{III} complexes **1(-)** (dash green line) and **1(+)** (full green line).

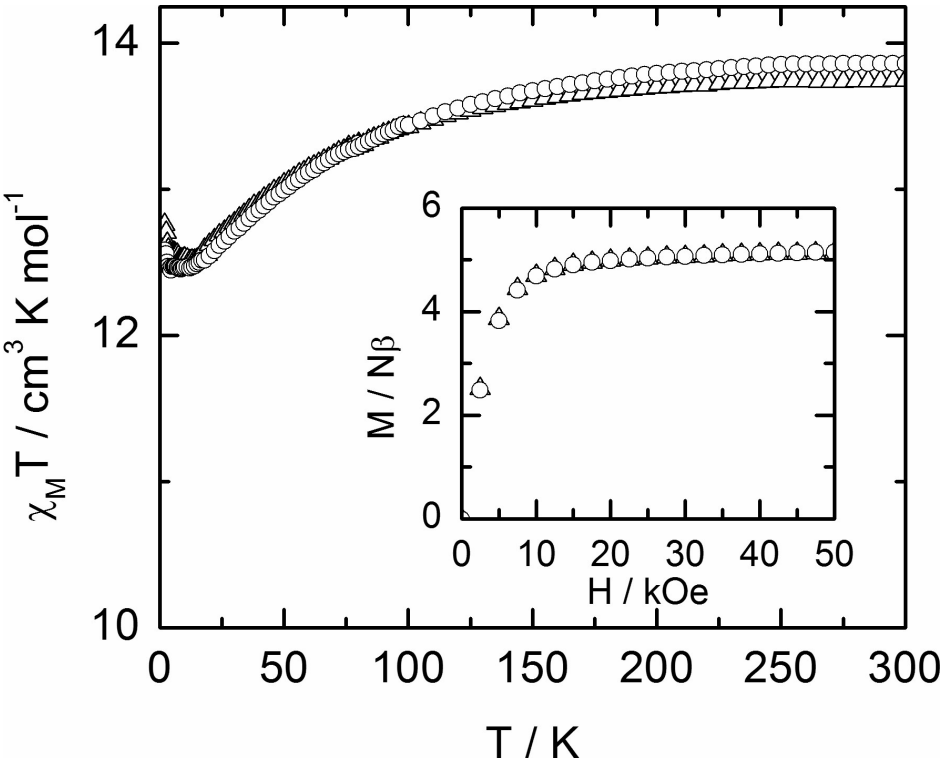

Figure S6. Temperatures dependences of $\chi_M T$ for **1(+)** (circles) and **1(-)** (triangles). In inset the field variations of the magnetization at 2 K.

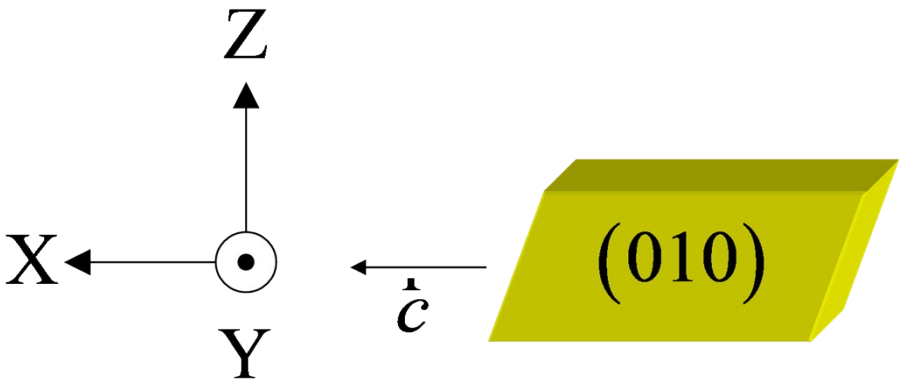

Figure S7. Oriented single crystal of *rac*-**1**·0.5C_6H_{14} with the XYZ crystal reference frame.

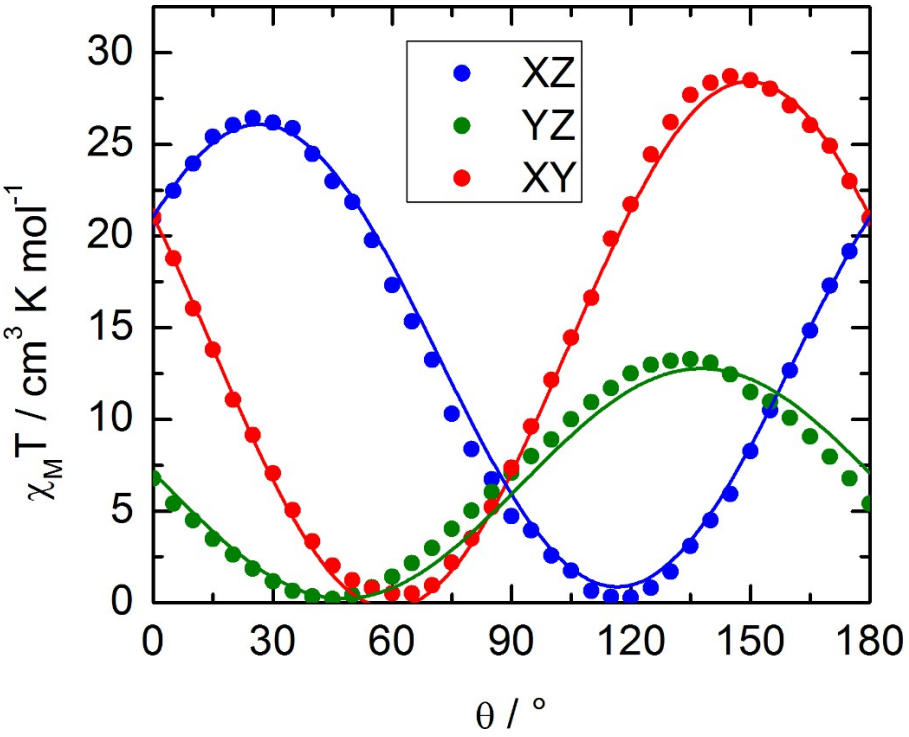

Figure S8. Angular dependence of $\chi_M T$ of a single crystal rotated of *rac*-**1**·0.5C_6H_{14} in the three perpendicular planes XY, XZ and YZ with H = 1 kOe at 2 K. Best fitted curves in full lines (see here below).

Molar magnetic susceptibility was fitted with:

$$\chi_M T = \frac{MT}{H} = \chi_{\alpha\alpha} \cos^2\theta + \chi_{\beta\beta} \sin^2\theta + 2\chi_{\alpha\beta} \sin\theta\cos\theta$$

where α and β are the directions X, Y and Z and θ is the angle between H and α.

After simultaneous least-square fitting of the three curves on Figure S7 the susceptibility tensor in the crystal frame (XYZ) is:

$$\chi_M T = \begin{pmatrix} 21.05 & -12.54 & 10.09 \\ -12.54 & 7.087 & -6.242 \\ 10.09 & -6.242 & 5.912 \end{pmatrix} \text{cm}^3 \text{ K mol}^{-1}$$

Principal values and direction of the susceptibility tensor in the XYZ crystal frame:

$$\chi_{xx} T \begin{pmatrix} 0.427 \\ 0.883 \\ 0.192 \end{pmatrix} = -0.341,\ \chi_{yy} T \begin{pmatrix} 0.439 \\ -0.016 \\ -0.898 \end{pmatrix} = 0.869,\ \chi_{zz} T \begin{pmatrix} 0.790 \\ -0.468 \\ 0.394 \end{pmatrix} = 33.52 \text{ cm}^3 \text{ K mol}^{-1}$$

Table S3. Computed energies levels (the ground state is set at zero), component values of the Lande factor *g* and wavefunction composition for each M_J state of the ground-state multiplet for *rac*-**1** in *rac*-**1**·0.5C_6H_{14}.

	Energy (cm^{-1})	g_x	g_y	g_z	Wavefunction composition
1	0.0	0.02	0.04	19.78	0.99|±15/2>
2	104.5	0.08	0.10	19.40	0.28|±1/2>+0.26|±3/2>+0.20|±5/2>+0.14|±7/2>
3	175.2	0.91	1.10	16.26	0.86|±13/2>
4	216.4	2.40	4.70	11.03	0.46|±11/2>+0.25|±9/2>
5	243.0	3.58	4.90	9.79	0.24|±9/2>+0.27|±7/2>+0.14|±11/2>+0.15|±1/2>
6	306.3	0.85	1.79	14.74	0.33|±9/2>+0.29|±7/2>+0.23|±11/2>
7	342.4	0.68	2.88	15.01	0.38|±5/2>+0.26 |±3/2>+0.17|±7/2>
8	723.2	0.00	0.00	19.82	0.43|±1/2>+0.31|±3/2>+0.16|±5/2>

Table S4. Computed energies levels (the ground state is set at zero), component values of the Lande factor *g* and wavefunction composition for each M_J state of the ground-state multiplet for **1(+)**.

	Energy (cm^{-1})	g_x	g_y	g_z	Wavefunction composition
1	0.0	0.01	0.01	19.66	0.97|±15/2>
2	103.6	0.71	2.09	16.68	0.23|±3/2>+0.20|±1/2>+0.20|±5/2>+0.16|±7/2>
3	159.5	0.93	2.93	11.97	0.52|±13/2>+0.15|±9/2>
4	198.1	9.16	6.25	1.84	0.29|±11/2>+0.21|±7/2>+0.15|±13/2>
5	244.4	2.21	3.04	13.23	0.29|±9/2>+0.28|±11/2>+0.15|±7/2>
6	302.3	2.44	4.42	10.50	0.33|±9/2>+0.15|±7/2>+0.15|±5/2>
7	331.2	1.19	6.22	12.08	0.26|±5/2>+0.23|±7/2>+0.16|±3/2>
8	582.3	0.00	0.01	19.72	0.47|±1/2>+0.31|±3/2>

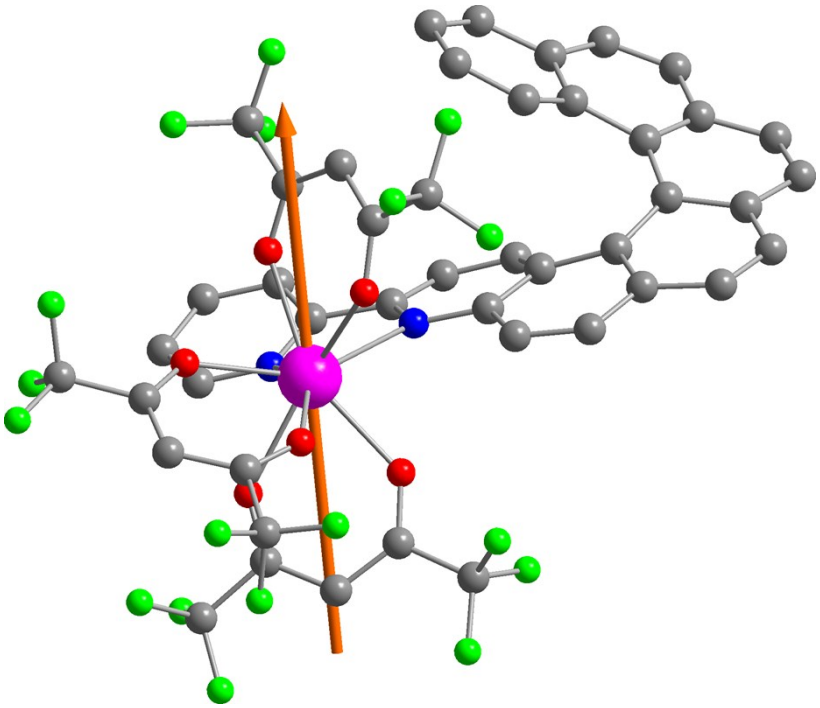

Figure S9. Representation of the crystallographic structure of **1(+)** (H atoms are omitted for clarity) with theoretical main anisotropy axis.

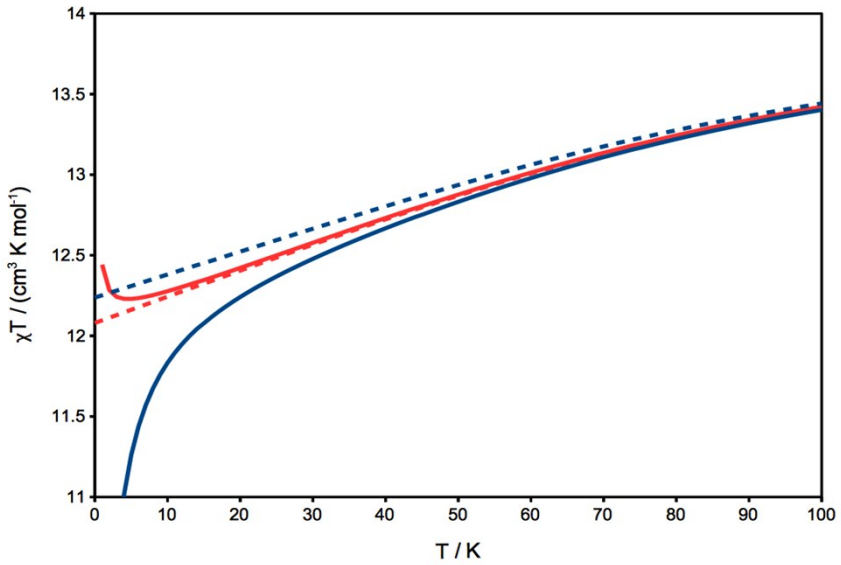

Figure S10. *Ab initio* computed temperature dependence of $\chi_M T$ between 0 and 100 K for *rac*-**1** (blue lines) and **1(+)** (red lines). Dotted lines show the $\chi_M T$ in absence of J_{dip}, while full lines include the calculated dipolar coupling.

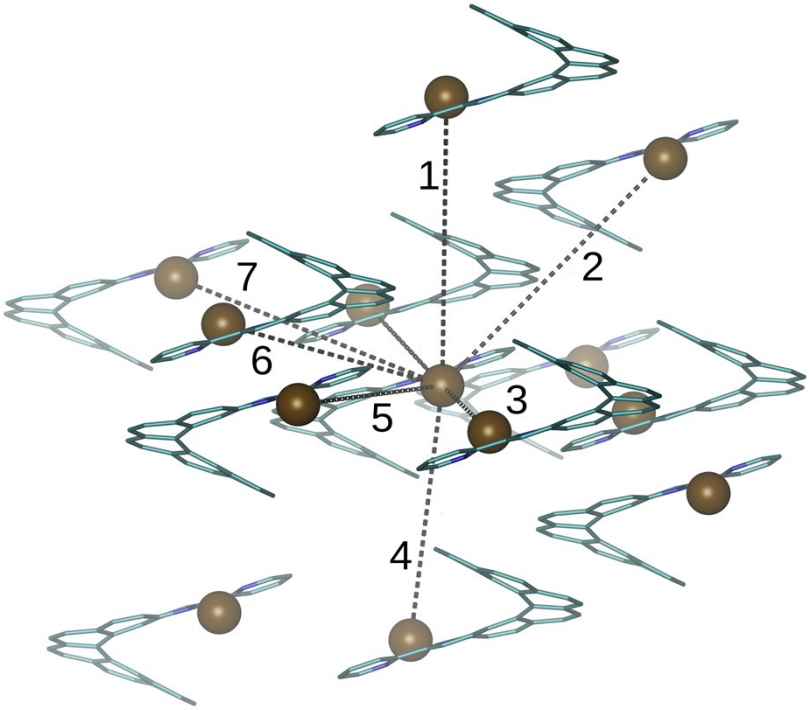

Figure S11. Schematic representation of the various dipolar coupling channels in *rac*-**1**·0.5C_6H_{14}. Corresponding J_{dip} values are given in Table S5.

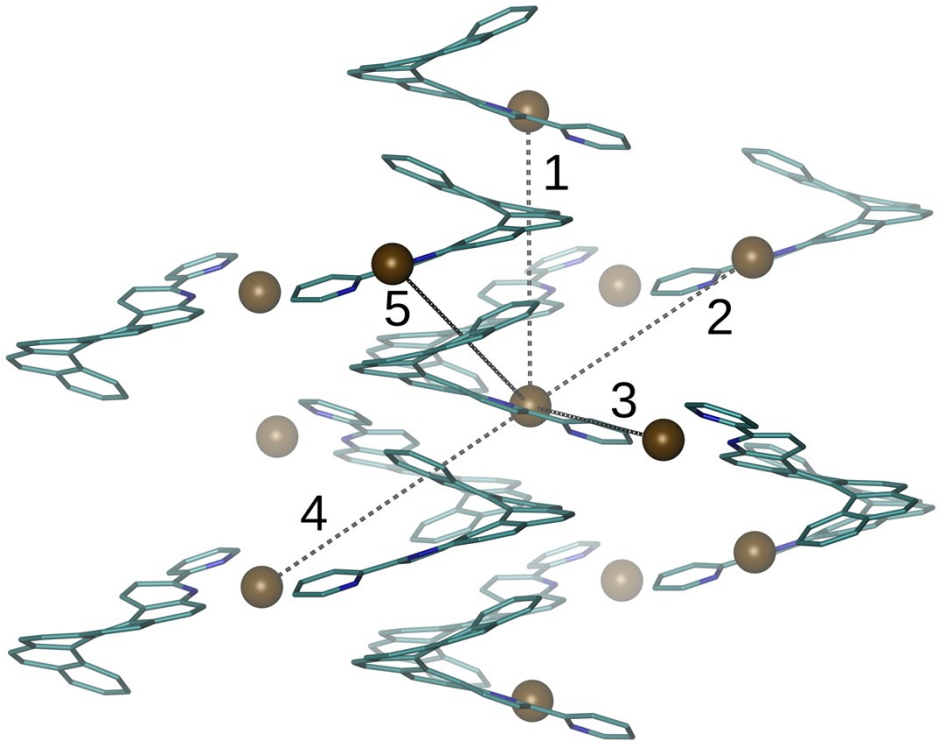

Figure S12. Schematic representation of the various dipolar coupling channels in **1(+)**. Corresponding J_{dip} values are given in Table S5.

Table S5. Calculated dipolar coupling values (in cm^{-1}) for the main pathways for *rac*-**1**·0.5C_6H_{14} (see Figure S10) and **1(+)** (see Figure S11). Average J_{dip} values are also given.

	rac-**1**·0.5C_6H_{14}	**1(+)**
1	0.11	0.19
2	-0.04	0.03
3	-0.20	0.09
4	0.18	-0.22
5	0.03	0.03
6	0.09	
7	-0.06	
J_{dip}	-0.055	0.0033

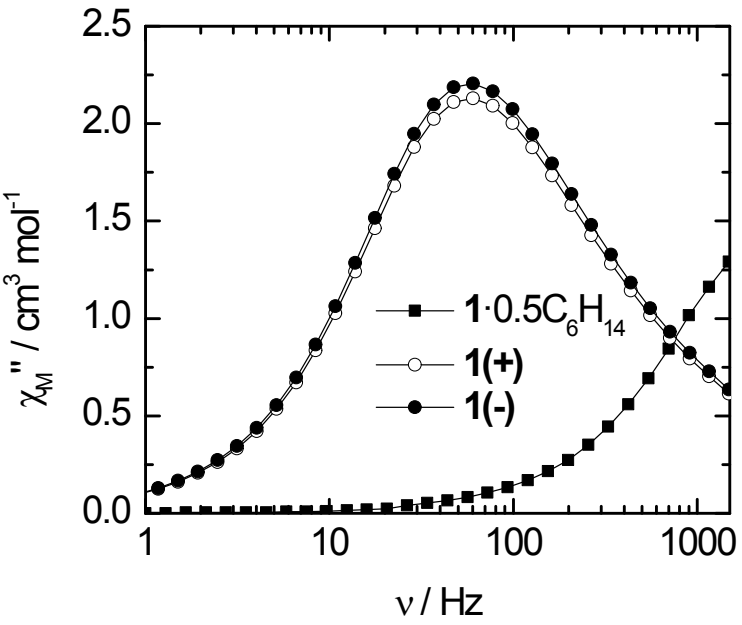

Figure S13. Frequency dependences of the out-of-phase component of the ac susceptibility, χ_M'', at 2 K measured in the absence of external dc field for *rac*-**1**·0.5C_6H_{14}, **1(+)** and **1(-)**.

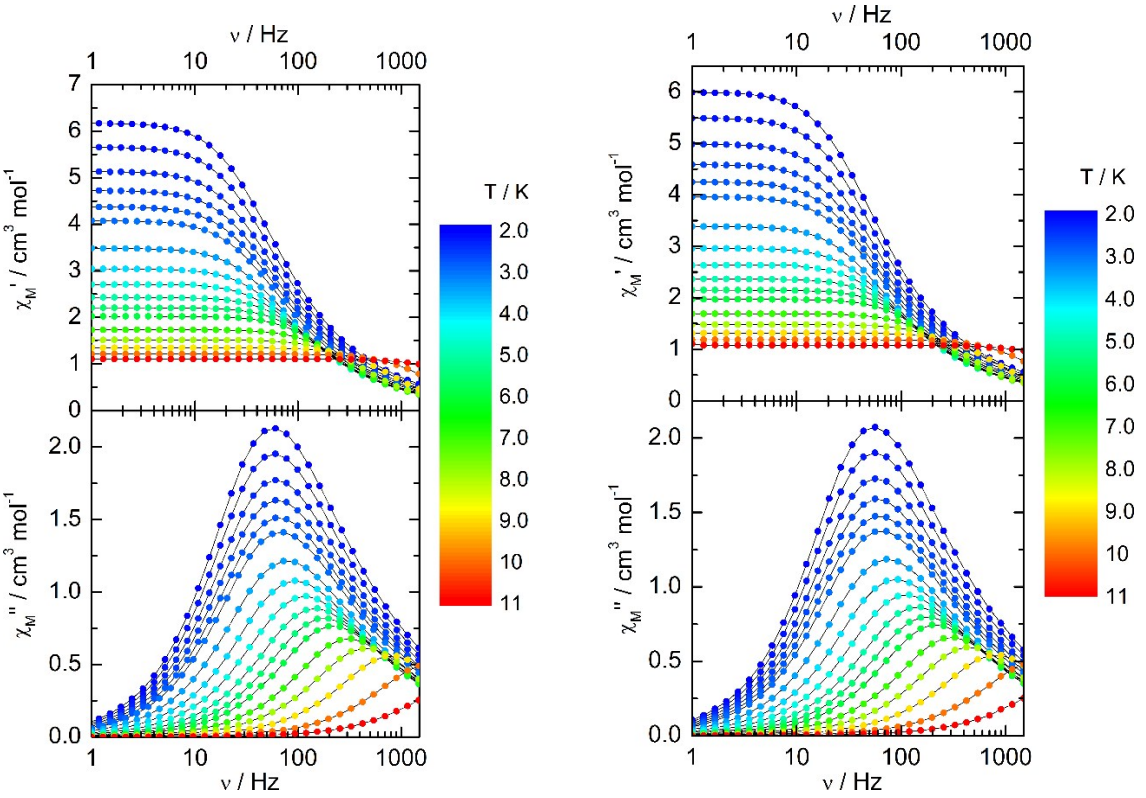

Figure S14. Frequency dependences of the in-phase, χ_M' (top), and out-of-phase, χ_M'' (bottom), components of the ac susceptibility between 2 and 11 K for **1(-)** (left) and **1(+)** (right) measured at zero external dc field.

Extended Debye model.

$$\chi' = \chi_S + (\chi_T - \chi_S)\frac{1+(\omega\tau)^{1-\alpha}\sin\left(\alpha\frac{\pi}{2}\right)}{1+2(\omega\tau)^{1-\alpha}\sin\left(\alpha\frac{\pi}{2}\right)+(\omega\tau)^{2-2\alpha}}$$

$$\chi'' = (\chi_T - \chi_S)\frac{(\omega\tau)^{1-\alpha}\cos\left(\alpha\frac{\pi}{2}\right)}{1+2(\omega\tau)^{1-\alpha}\sin\left(\alpha\frac{\pi}{2}\right)+(\omega\tau)^{2-2\alpha}}$$

With χ_T the isothermal susceptibility, χ_S the adiabatic susceptibility, τ the relaxation time and α the empiric parameter which describes the distribution of the relaxation time. For SMM with only one relaxing object α is close to zero. The extended Debye model was applied to fit simultaneously the experimental variations of χ_M' and χ_M'' with the frequency f of the oscillating field ($\omega = 2\pi f$). Typically, only the temperatures for which a maximum on the χ_M'' vs. f curves have been considered (see figure here below for an example). The best fitted parameters τ, α, χ_T, χ_S are listed in tables here below with the coefficient of determination R^2.

Table S6. Best fitted parameters (χ_T, χ_S, τ and α) with the extended Debye model for **1(+)** at 0 Oe in the temperature range 2-10 K.

T / K	χ_T / cm^3 mol^{-1}	χ_S / cm^3 mol^{-1}	A	τ / s	R²
2	6.14589	0.46922	0.19488	0.00237	0.99858
2.2	5.63111	0.43365	0.19404	0.00233	0.99858
2.4	5.11026	0.40238	0.1922	0.00227	0.99859
2.6	4.69973	0.37111	0.19123	0.0022	0.9986
2.8	4.3522	0.34749	0.18958	0.00212	0.9986
3	4.05399	0.32551	0.18786	0.00203	0.99864
3.5	3.4597	0.29868	0.17933	0.00176	0.99867
4	3.01634	0.2895	0.1632	0.00147	0.99879
4.5	2.67889	0.27133	0.14921	0.00119	0.99889
5	2.39349	0.27313	0.127	9.71E-04	0.99923
5.5	2.17094	0.26081	0.11061	8.00E-04	0.99939
6	1.9863	0.24816	0.09523	6.71E-04	0.99954
7	1.69859	0.21939	0.07048	4.87E-04	0.99977
8	1.48369	0.18948	0.05063	3.44E-04	0.9999
9	1.31687	0.15931	0.03938	1.99E-04	0.99997
10	1.18567	0.13039	0.04643	8.50E-05	0.99999

Table S7. Best fitted parameters (χ_T, χ_S, τ and α) with the extended Debye model for **1(-)** at 0 Oe in the temperature range 2-10 K.

T / K	χ_T / cm^3 mol^{-1}	χ_S / cm^3 mol^{-1}	α	τ / s	R²
2	6.25388	0.50021	0.18382	0.00223	0.99899
2.2	5.73348	0.46185	0.18363	0.00219	0.99901
2.4	5.20096	0.42019	0.18283	0.00212	0.99899
2.6	4.78435	0.39283	0.18122	0.00206	0.999
2.8	4.42932	0.36766	0.18007	0.00198	0.99902
3	4.16916	0.32958	0.19005	0.00192	0.99869
3.5	3.5575	0.3029	0.18122	0.00167	0.99874
4	3.10039	0.29517	0.16468	0.0014	0.99884
4.5	2.75422	0.27924	0.15086	0.00115	0.99891
5	2.45999	0.27746	0.12838	9.40E-04	0.99922
5.5	2.23067	0.26507	0.11169	7.80E-04	0.9994
6	2.04047	0.25184	0.09605	6.57E-04	0.99955
7	1.74452	0.22097	0.07107	4.78E-04	0.99975

8	1.52353	0.19269	0.05112	3.40E-04	0.99991
9	1.35221	0.15569	0.03955	1.97E-04	0.99998
10	1.21743	0.14436	0.0436	8.60E-05	0.99999

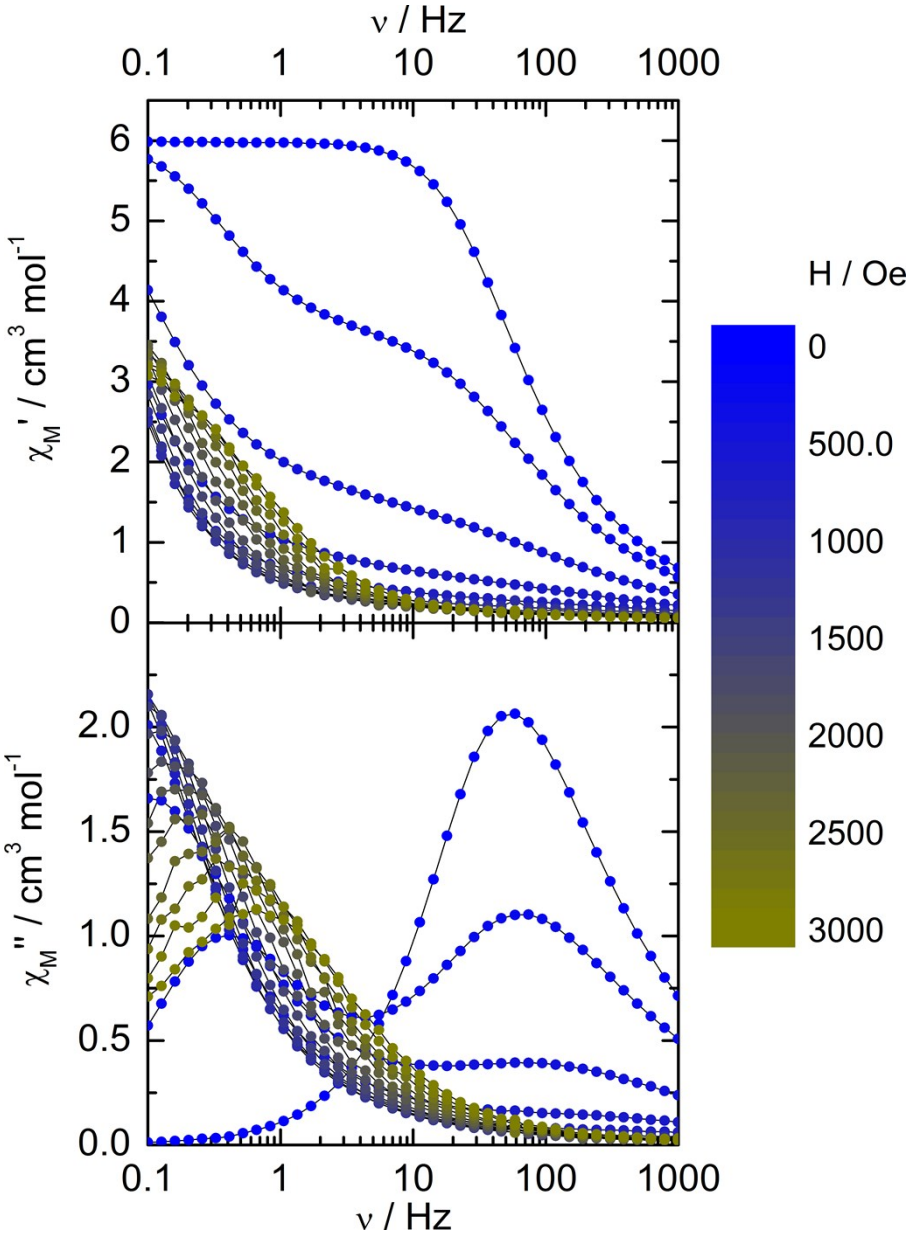

Figure S15. Frequency dependences of the in-phase, χ_M' (top), and out-of-phase, χ_M'' (bottom), components of the ac susceptibility at 2 K for **1(+)** as a function of the external dc field.

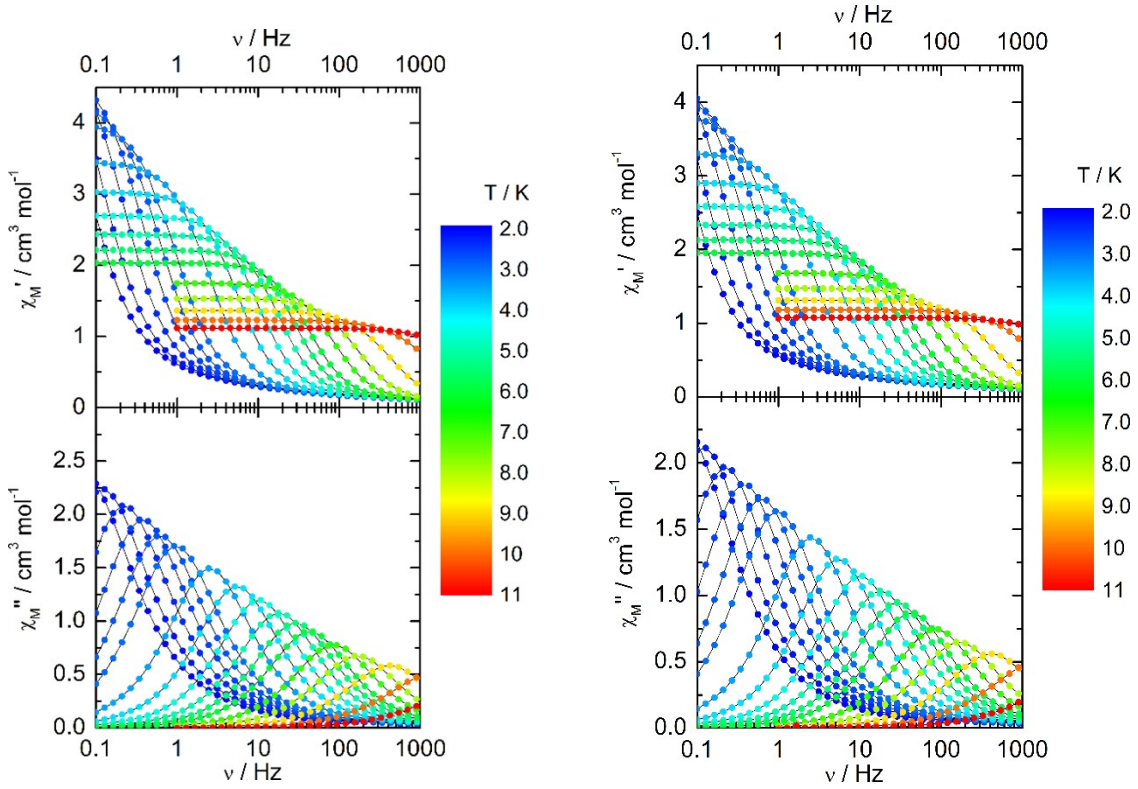

Figure S16. Frequency dependences of the in-phase, χ_M' (top), and out-of-phase, χ_M'' (bottom), components of the ac susceptibility between 2 and 11 K for **1(-)** (left) and **1(+)** (right) measured at 1 kOe.

Table S8. Best fitted parameters (χ_T, χ_S, τ and α) with the extended Debye model for **1(+)** at 1 kOe in the temperature range 2-10 K.

T / K	χ_T / cm^3 mol^{-1}	χ_S / cm^3 mol^{-1}	α	τ / s	R^2
2	8.11525	0.17718	0.27621	4.10301	0.99562
2.2	6.19468	0.17773	0.21121	1.62892	0.99675
2.4	5.14851	0.17576	0.15562	0.73827	0.99774
2.6	4.60417	0.16893	0.12513	0.41423	0.99843
2.8	4.21454	0.16284	0.10534	0.25079	0.9989
3	3.90689	0.15738	0.09111	0.16033	0.9992
3.5	3.33199	0.14628	0.06948	0.06208	0.99965
4	2.9174	0.13696	0.05555	0.02881	0.99984
4.5	2.59334	0.12804	0.04463	0.01544	0.99988
5	2.33858	0.11871	0.04313	0.00885	0.99997
5.5	2.13082	0.10932	0.0408	0.00556	0.99996
6	1.9553	0.10371	0.03889	0.00372	0.99998
7	1.68262	0.09326	0.03908	1.87E-03	0.99998
8	1.47467	0.08415	0.04377	9.55E-04	0.99998
9	1.31242	0.06683	0.06566	3.90E-04	0.99999
10	1.18297	0.02224	0.1102	1.13E-04	0.99998

Table S9. Best fitted parameters (χ_T, χ_S, τ and α) with the extended Debye model for **1(-)** at 1 kOe in the temperature range 2-10 K.

T / K	χ_T / cm^3 mol^{-1}	χ_S / cm^3 mol^{-1}	α	τ / s	R^2
2	8.88955	0.18188	0.28977	4.28414	0.99567
2.2	6.63483	0.18678	0.21929	1.6126	0.99664
2.4	5.49371	0.18677	0.16099	0.73007	0.99757
2.6	4.90716	0.18127	0.12888	0.41025	0.9983
2.8	4.41078	0.17437	0.10827	0.24938	0.9988
3	4.0822	0.16807	0.09483	0.1594	0.99912
3.5	3.47757	0.15801	0.07029	0.06171	0.9996
4	3.04025	0.14879	0.05592	0.02864	0.99984
4.5	2.70352	0.13814	0.04569	0.01539	0.99986
5	2.43672	0.12868	0.04328	0.00881	0.99997
5.5	2.21796	0.11946	0.04014	0.00554	0.99998
6	2.03605	0.10869	0.03938	0.00369	0.99998
7	1.7512	0.09906	0.03786	1.86E-03	0.99999
8	1.53493	0.08993	0.04184	9.51E-04	0.99999
9	1.36495	0.07197	0.06502	3.87E-04	0.99998
10	1.23104	0.0268	0.11079	1.13E-04	0.99999

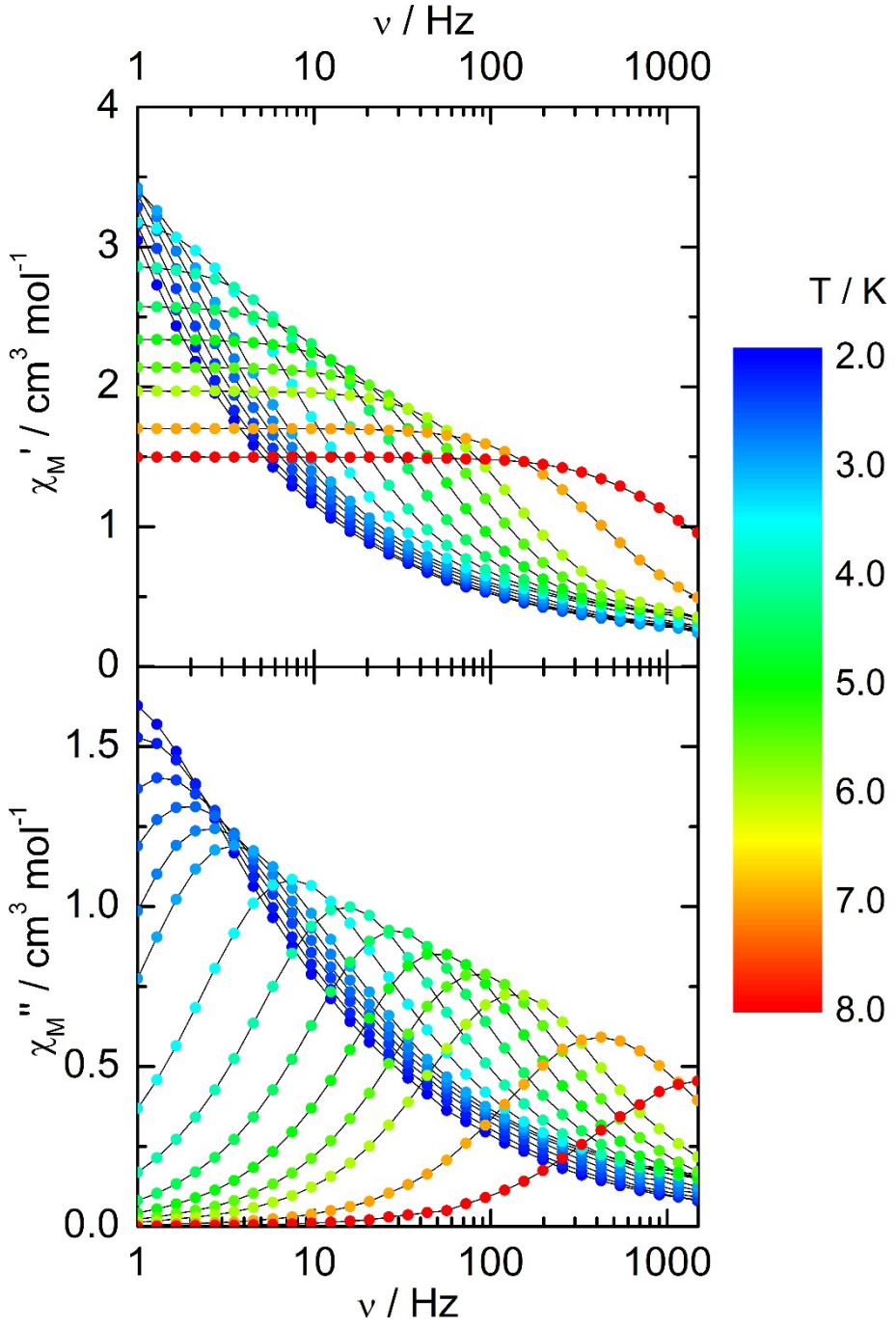

Figure S17. Frequency dependences of the in-phase, χ_M' (top), and out-of-phase, χ_M'' (bottom), components of the ac susceptibility between 2 and 8 K for *rac*-**1**·0.5C_6H_{14} measured at 1 kOe.

Table S10. Best fitted parameters (χ_T, χ_S, τ and α) with the extended Debye model for **1**·0.5C_6H_{14} at 1 kOe in the temperature range 2-8 K.

T / K	χ_T / cm^3 mol^{-1}	χ_S / cm^3 mol^{-1}	α	τ / s	R^2
2	8.62086	0.23959	0.47454	0.50976	0.9995
2.2	7.4378	0.22828	0.46179	0.30765	0.99927
2.4	6.32779	0.22755	0.44172	0.17253	0.99878
2.6	5.55667	0.23674	0.41934	0.10578	0.99815
2.8	4.9242	0.25371	0.38983	0.06692	0.99719
3	4.38714	0.28278	0.35067	0.04339	0.9964
3.5	3.49691	0.34665	0.25056	0.01811	0.9964
4	2.98133	0.3726	0.17657	0.0091	0.99784
4.5	2.62888	0.37061	0.13023	0.00499	0.999
5	2.36829	0.35409	0.10463	0.00292	0.99949
5.5	2.15779	0.33666	0.08871	0.00178	0.99968
6	1.98315	0.32184	0.08224	0.0011	0.99978
7	1.71005	0.3076	0.10012	3.72E-04	0.99987
8	1.5005	0.43115	0.10942	1.14E-04	0.99996

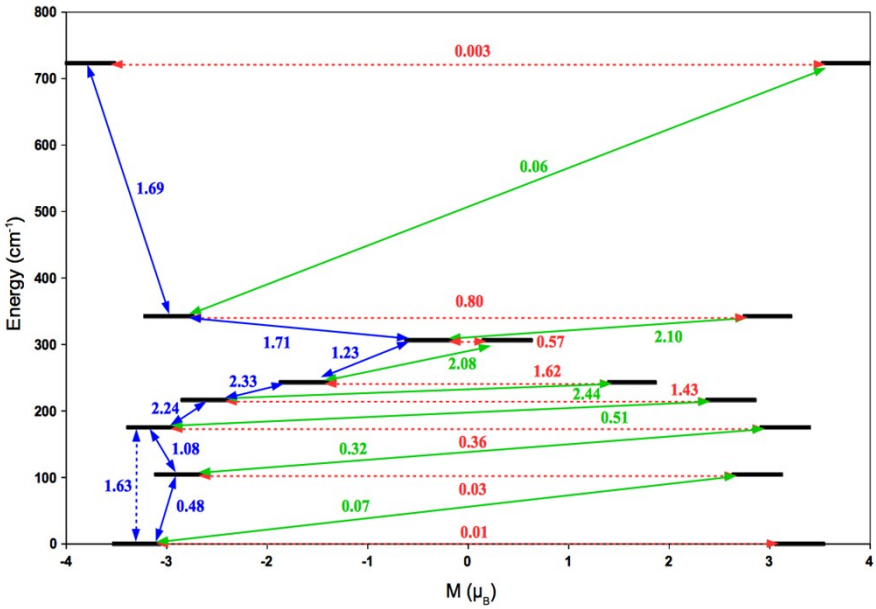

Figure S18. *Ab initio* magnetization blocking barrier for *rac*-**1**, computed by means of magnetic transition moments. The black thick lines correspond to all the spin–orbit states. The full green lines shows possible Orbach processes, dotted red lines quantum tunneling processes, full blue lines direct vertical transitions to the first-neighbor multiplet, dotted blue lines direct vertical transitions to the second-neighbor multiplet.

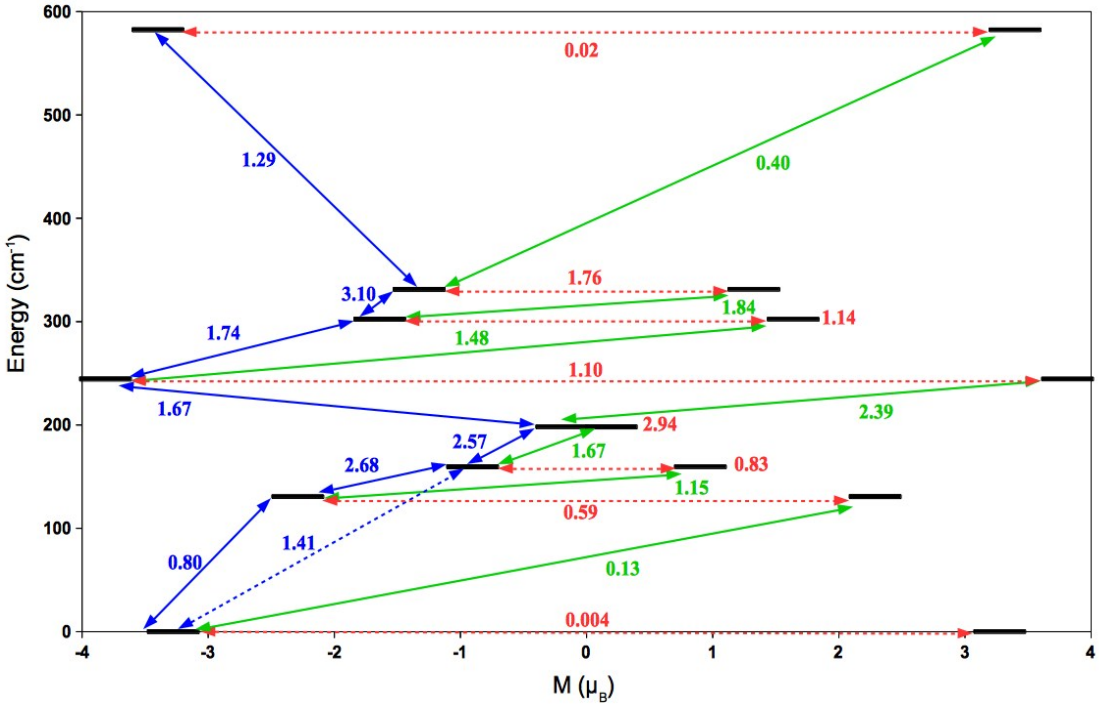

Figure S19. *Ab initio* magnetization blocking barrier for **1(+)**, computed by means of magnetic transition moments. The black thick lines correspond to all the spin–orbit states. The full green lines shows possible Orbach processes, dotted red lines quantum tunneling processes, full blue lines direct vertical transitions to the first-neighbor multiplet, dotted blue lines direct vertical transitions to the second-neighbor multiplet.

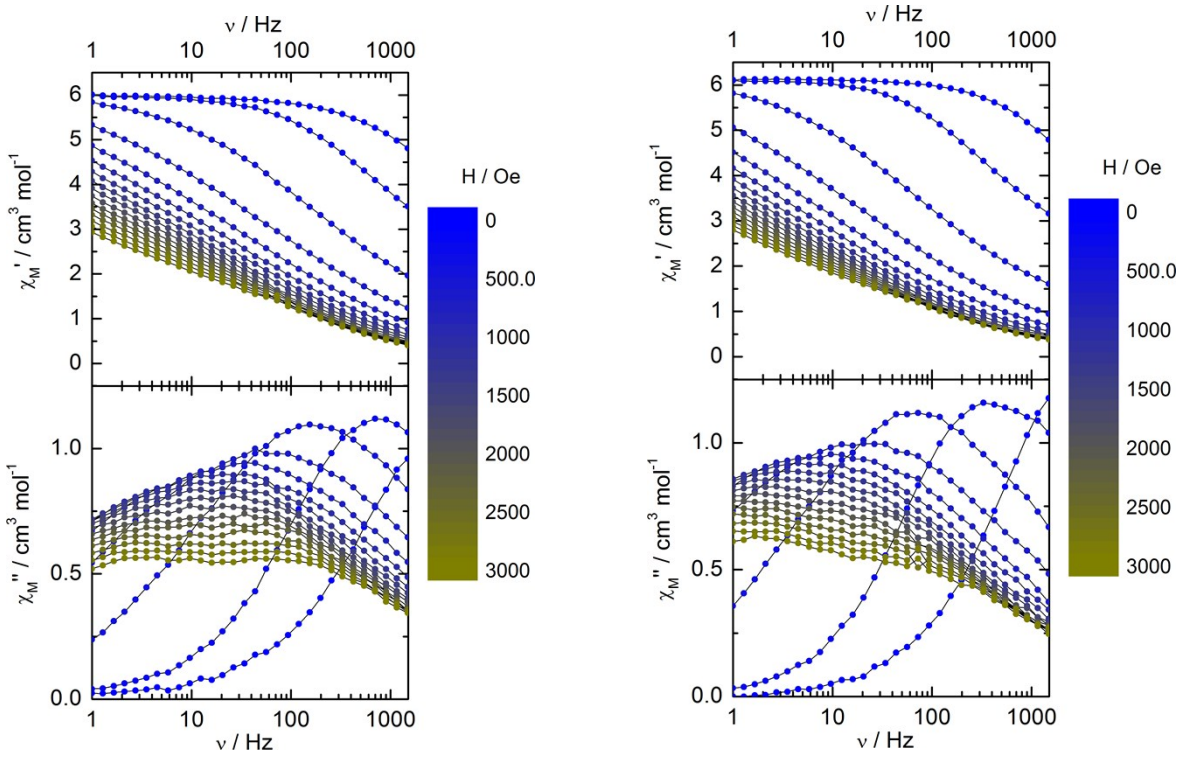

Figure S20. Frequency dependences of the in-phase, χ_M' (top), and out-of-phase, χ_M'' (bottom), components of the ac susceptibility at 2 K between 0 and 3000 Oe for dichloromethane solutions of *rac*-**1** (left) and **1(+)** (right).

References

(1) M. F. Richardson, W. F. Wagner, D. E. Sands, *J. Inorg. Nucl. Chem.*, 1968, **30**, 1275.

(2) (a) N. Saleh, M. Srebro, T. Reynaldo, N. Vanthuyne, L. Toupet, V. Y. Chang, G. Muller, J. A. G. Williams, C. Roussel, J. Autschbach, J. Crassous, *Chem. Commun.*, 2015, **51**, 3754; (b) N. Saleh, B. Moore, II, M. Srebro, N. Vanthuyne, L. Toupet, J. A. G. Williams, C. Roussel, K. K. Deol, G. Muller, J. Autschbach, J. Crassous, *Chem. Eur. J.*, 2015, **21**, 1673.

(3) SHELX97 - Programs for Crystal Structure Analysis (Release 97-2). G. M. Sheldrick, Institut für Anorganische Chemie der Universität, Tammanstrasse 4, D-3400 Göttingen, Germany, 1998. SIR97 – A. Altomare, M. C. Burla, M. Camalli, G. L. Cascarano, C. Giacovazzo, A. Guagliardi, A. G. G. Moliterni, G. Polidori, R. Spagna, *J. Appl. Cryst.*, 1999, **32**, 115.

(4) F. Aquilante, L. De Vico, N. Ferré, G. Ghigo, P.-A. Malmqvist, P. Neogrady, T. B. Pedersen, M. Pitonak, M. Reiher, B. O. Roos, L. Serrano-Andrés, M. Urban, V. Veryazov, R. Lindh, *J. Comput. Chem.*, 2010, **31**, 224.

(5) B. O. Roos, P. R. Taylor, P. E. M. Siegbahn, *Chem. Phys.*, 1980, **48**, 157.

(6) (a) P.-A. Malmqvist, B. O. Roos, B. Schimmelpfennig, *Chem. Phys. Lett.*, 2002, **357**, 230. (b) P.-A. Malmqvist, B. O. Roos, *Chem. Phys. Lett.*, 1989, **155**, 189.

(7) (a) L. F. Chibotaru, L. Ungur, *J. Chem. Phys.*, 2012, **137**, 064112; (b) L. F. Chibotaru, L. Ungur, A. Soncini, *Angew. Chem., Int. Ed.*, 2008, **47**, 4126.

(8) F. Aquilante, P.-A. Malmqvist, T. B. Pedersen, A. Ghosh, B. O. Roos, *J. Chem. Theory Comput.*, 2008, **4**, 694.

(9) (a) B. O. Roos, R. Lindh, P.-A. Malmqvist, V. Veryazov, P.-O. Widmark, *J. Phys. Chem. A*, 2004, 108, 2851; (b) B. O. Roos, R. Lindh, P.-A. Malmqvist, V. Veryazov, P.-O. Widmark, *J. Phys. Chem. A*, 2005, **109**, 6576; (c) B. O. Roos, R. Lindh, P.-A. Malmqvist, V. Veryazov, P.-O. Widmark, A.-C. Borin, *J. Phys. Chem. A*, 2008, **112**, 11431.

(10) M. J. Frisch, G. W. Trucks, H. B. Schlegel, G. E. Scuseria, M. A. Robb, J. R. Cheeseman, G. Scalmani, V. Barone, B. Mennucci, G. A. Petersson, H. Nakatsuji, M. Caricato, X. Li, H. P. Hratchian, A. F. Izmaylov, J. Bloino, G. Zheng, J. L. Sonnenberg, M. Hada, M. Ehara, K. Toyota, R. Fukuda, J. Hasegawa, M. Ishida, T. Nakajima, Y. Honda, O. Kitao, H. Nakai, T. Vreven, J. A. Montgomery, Jr., J. E. Peralta, F. Ogliaro, M. Bearpark, J. J. Heyd, E. Brothers, K. N. Kudin, V. N. Staroverov, R. Kobayashi, J. Normand, K. Raghavachari, A. Rendell, J. C. Burant, S. S. Iyengar, J. Tomasi, M. Cossi, N. Rega, J. M. Millam, M. Klene, J. E. Knox, J. B. Cross, V. Bakken, C. Adamo, J. Jaramillo, R. Gomperts, R. E. Stratmann, O. Yazyev, A. J.

Austin, R. Cammi, C. Pomelli, J. W. Ochterski, R. L. Martin, K. Morokuma, V. G. Zakrzewski, G. A. Voth, P. Salvador, J. J. Dannenberg, S. Dapprich, A. D. Daniels, Ö. Farkas, J. B. Foresman, J. V. Ortiz, J. Cioslowski, and D. J. Fox Gaussian 09, Revision A.02; Gaussian Inc.: Wallingford, CT, 2009.

(11) (a) J. P. Perdew, K. Burke, M. Ernzerhof, *Phys. Rev. Lett.*, 1996, **77**, 3865; (b) C. Adamo, V. Barone, *J. Chem. Phys.*, 1999, **110**, 6158.

(12) M. Dolg, H. Stoll, H. Preuss, *Theor. Chim. Acta*, 1993, **85**, 441.

(13) F. Weigend, R. Ahlrichs, *Phys. Chem. Chem. Phys.*, 2005, **7**, 3297.

(14) Electron Paramagnetic Resonance of Exchange Coupled Systems, A. Bencini, D. Gatteschi, 1990, Springer.